Low-Power Ultrasonic Front-End for Cargo Container Monitoring

J. M. Algueta-Miguel, J. R. Garcia-Oya, A. J. Lopez-Martin, *Senior Member, IEEE,* C. A. De La Cruz Blas, *Member, IEEE,* F. Muñoz Chavero, *Member, IEEE* and E. Hidalgo-Fort

***Abstract*— A low-power ultrasonic communication front-end conceived for cargo container monitoring is presented. Two piezoelectric transducers operating at 40 kHz are fixed to the metallic wall by means of a customized magnetic case, allowing a non-invasive inside-outside communication preserving the container integrity. Once the resulting ultrasonic channel is characterized, an experimental measurement setup based on FPGA is implemented for testing some basic modulation and detection schemes in terms of Bit Error Rate (BER), also considering their robustness against undesired mechanical and electromagnetic perturbations. On this basis, a compact digital DBPSK modulator using a square carrier signal is proposed. Frequency and amplitude tracking algorithms are designed for optimizing the quality and robustness of the data transmission. Finally, a low-power low-rate (up to few kbps) architecture based on the previous elements is presented. All the proposed contributions are experimentally validated.**

***Index Terms* — Data acquisition, cargo-container monitoring, ultrasonics, ultrasonic front-end, through-metal communication, BER measurement, piezoelectric transducers, charge amplifier.**

I. Introduction

THE vertiginous growth of worldwide freight transportation over the last two decades has motivated an intensive research in smart monitoring of cargo containers, aimed at improving efficiency, safety, security and sustainability [1-4]. Commonly, the internal data of the container are acquired by a sensor network [5] and, once outside the container, this information is transmitted through a wireless network for subsequent processing [6, 7]. In this context, this work is focused on the inside-outside interface that delivers the internal data to the external wireless node through the container wall. Several non-invasive methods have been employed for wireless through-metal communication [8-10]. From an electromagnetic viewpoint, inductive coupling [9, 11, 12] and near-field devices [13] have been used for transmitting energy through metal walls, but their low efficiency makes them unsuitable for data transmission. In this scenario, ultrasonic acoustic waves are considered the most efficient choice for data and/or power transfer through metallic barriers.

Electromagnetic-acoustic transducers (EMATs) [9, 14] and piezoelectric transducers (PTs) [15-26] are the most popular devices for this approach. The strength of EMATs lies in their capability of non-contact operation. However, PTs are the most popular choice due to their higher efficiency, in spite of requiring an accurate coupling [16].

Typically, thick metal barriers have to be overcome and/or a high-rate highly robust transmission is aimed, so multi-carrier data multiplexing becomes a very common approach. Orthogonal Frequency Division Multiplexing (OFDM) is by far the most common choice [17-20], usually including empirical equalization schemes based on feedback algorithms. However, previous works addressing in depth low-power through-wall ultrasonic communication in general [22] and regarding cargo container monitoring in particular, are only marginally covered in the literature [24, 25].

In this context, a versatile non-invasive ultrasonic front-end for data transmission through the container wall is presented in this work. It follows a low-cost, low-rate and low-power approach, clearly improving the transmission power requirements of any of the related proposals [22, 24, 25].

A reversible and non-invasive placement system of PTs is presented in Section II. It is based on a magnetic case specifically designed for this application, both safeguarding the integrity of the container and facilitating the transducer installation. The channel characterization using this transducer fixation method is performed. Moreover, several modulation schemes defined in Section III have been tested in terms of Bit Error Rate (BER) in Section IV. A FGPA-based measurement system [27] has been designed for this purpose. Also, electrical and mechanical perturbations have been applied for evaluating the robustness of the different modulations, which has not been previously reported in the literature to the best of the authors' knowledge.

On this basis, a novel Differential Binary Phase Shift Keying (DBPSK) modulator based on a digitally-generated square carrier signal is proposed in Section V. In order to optimize the quality and robustness of the data transmission, frequency and tracking algorithms are presented in Section VI. A pseudo-differential charge amplifier [28] providing sensitivity programmability is employed for signal conditioning. A final architecture based on the previous contributions is implemented under simplicity and low-power criteria in Section VII, since a low data rate (of one or few

This work was supported in part by Spanish Agencia Estatal de Investigación and Fondo Europeo de Desarrollo Regional under Grant TEC2016-80396-C2-1-R, and in part by the Obra Social La Caixa, Fundación Caja Navarra (Convocatoria 2018 de Captación de Talento).

J. M. Algueta-Miguel, A. J. López-Martín and C. A. De la Cruz Blas are with the Smart Cities Institute, Public University of Navarra, Pamplona, E-31006 Spain (e-mail: {josemaria.algueta, antonio.lopez, carlos.aristoteles}@unavarra.es)

J. R. García-Oya, F. Muñoz Chavero and E. Hidalgo-Fort are with the Electronic Engineering Department, University of Seville, Sevilla, E-41092 Spain (e-mail: jose.garciaoya@gie.esi.us.es, {fmunoz, ehidalgo}@us.es)

kbps) clearly fulfills the requirements for container monitoring [25]. Finally, a brief conclusion is drawn in Section VIII.

II. Ultrasonic Transducer and Channel Characterization

According to the International Standards Organization (ISO), dimensions of shipping containers are 2.44 m (8 ft and 6 in) wide by 6.10 or 12.20 m (20 or 40 ft) long and 2.59 m (8 ft and 6 in) high. The walls are typically made of trapezoidal corrugated steel sheets, with a thickness of 1.8 or 2 mm. The exact size of the trapezoidal profile can vary according to the type of container and the installation place (long or front side). In order to model the container wall, a galvanized steel plate of 50 cm x 50 cm and 2 mm thickness was chosen for the laboratory tests. A layer of plastic paint was applied for a closer approximation to the real scenario.

A. Ultrasonic Transducer Selection

Concerning the ultrasonic piezoelectric transducer, the Prowave 400EP250 was chosen among several models due to its good tradeoff between sensitivity and cost. This device has a diameter of 25 mm and a nominal operation frequency of 40 kHz, which is clearly affordable for a low-rate communication. Furthermore, multipath due to diffraction effects on the transducer boundary can be minimized operating in the so called far field region [12], in which the resulting acoustic wave is approximately planar for wall thicknesses larger than $d^2/4\lambda$, where d is the PT diameter and λ is the wavelength of the acoustic signal. In this application, the previous condition is fulfilled by the chosen transducer at operation frequencies lower than 65 kHz.

B. Ultrasonic Transducer Installation

High-strength high-toughness adhesive is often used for permanently fixing PTs to metal structures [16-18, 20, 22] yielding good coupling properties and excellent physical resistance. Nevertheless, permanent adhesives require a drying time and both transducer and container can be damaged if they have to be separated. Moreover, aging deteriorates the adhesion performance. By contrast, a removable fixing is more versatile, allowing a quick and easy installation and preserving the integrity of both elements. However, the establishment of a robust communication becomes a challenging task in this latter case: the insufficient and irregular transducer-wall pressure as well as the deficient support due to the surface roughness, are typical harmful effects associated to a reversible fixing approach. A system based on magnetic enclosures was used in [25] for containing the whole communication system (PT transmitter/receiver modules) and protecting it from adverse environmental conditions, but the coupling quality between the transducer and the container wall was not a major concern.

In this context, the magnetic case design shown in Fig. 1 is proposed for optimizing the through-wall signal transmission. It consists of two plastic pieces fabricated with a 3-D printer. The 400EP250 transducer is fitted in one of them, which in turn includes 8 threaded and equally-spaced neodymium magnets around to hold the case on the steel wall, also producing a homogenous pressure on the PT. The second piece is a cover which is fixed to the magnets by means of screws, thus allowing them to graduate the prominence of the transducer over the base of the case. Also, a high density foam pad has been added between the transducer and the plastic cover, since it has been experimentally confirmed that a moderately elastic pad under compression enhances the adaptability to the metallic wall. The compression level of the foams can be adjusted by the clamping screws.

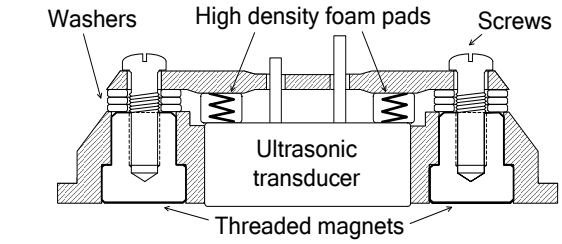

(a)

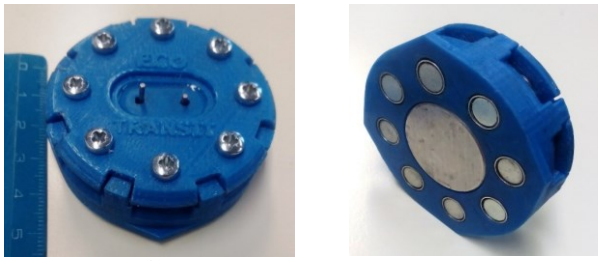
(b) (c)

Fig. 1. Fabricated magnetic case adapted to ultrasonic transducer 400EP250 (a) Scheme (b) Upper side photograph (c) Bottom side photograph.

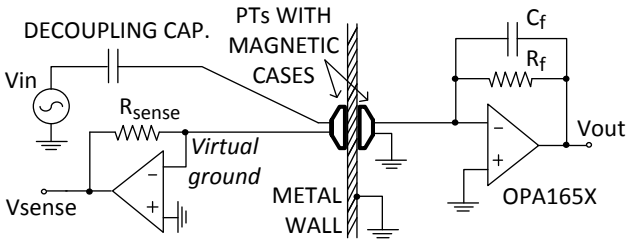

Fig. 2. Set-up for experimental characterization of ultrasonic channel.

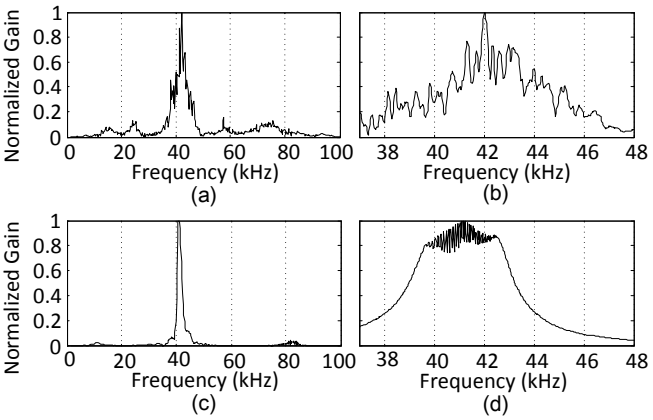

Fig. 3. Normalized frequency response of the ultrasonic channel: (a) Transducers attached using the magnetic cases (b) Detail of the frequency range of interest of (a) (c) Directly placing both transducers back to back, only for comparison. (d) Detail of the freq. range of interest of (c).

C. Channel Characterization

The scheme of Fig. 2 has been used for the experimental characterization of the ultrasonic channel. The classical charge amplifier topology based on a high input impedance (FET input) opamp and a feedback RC network has been selected to perform the charge-voltage conversion at the output [29]. A transresistance amplifier has been connected to the negative terminal of the transmitter PT for sensing the current through the input PT for characterization purposes. An electrical impedance of 2 kΩ (in magnitude) has been measured at the PT operation frequency using this system. Moreover, the metal wall has been kept grounded to avoid electrical coupling and thus ensuring a purely mechanical transmission. Under these conditions, the frequency response of the system of Fig. 2 has been measured using a network analyzer.

The obtained results are shown in Fig. 3, in which the normalized channel response of Fig. 3(a) (a zoom of the zone of interest is provided in Fig. 3(b)) is compared with the frequency response of both transducers directly connected back-to-back (Fig. 3(c), with zoom in Fig. 3(d)). Note that a highly selective frequency response with numerous peaks and valleys separated by a few hundred Hz is obtained. This is a typical behavior in through-wall ultrasonic channels (e.g. [18, 22, 24]) due to the acoustic impedance mismatch in the different interfaces that produces multiple reflections, leading to complex highly reverberant channels. Also, interference due to diffraction effects [9] can affect the characteristics of the channel, as previously explained.

Consequently, the envelope shape and the optimal transmission frequency of the spectra of Figs. 3(a) and 3(b) can significantly vary for each transducer placement due to the irregularities of the container wall. In order to statistically characterize the frequency for maximum power transmission (f_{MPT}), the placement of both transducers at different points of the steel plate has been monitored for 100 realizations. The obtained f_{MPT} varies from 38 kHz to 48 kHz, being between 41 kHz and 45 kHz for more than 75% of the cases.

Similarly, the effect of misalignment between transducers was also investigated but well reproducible results could not be obtained. Although a pattern of constructive and destructive interferences could be roughly deduced by progressively displacing one of the transducers in steps of 1 cm, strong variations were obtained for each experiment realization. Hence, one may conclude that the aforementioned variability associated to the transducer attachment clearly dominates over the effect of misalignments.

III. Basic Modulations and Detection Schemes

As mentioned in Section I, this work is focused on low-rate low-power communication (well suited to low-cost container monitoring), so simple modulation schemes based on different paradigms (amplitude, frequency and time position) with no equalization and low computational cost are explored. Specifically, the four basic modulations in Fig. 4, together with the detection schemes of Fig. 5, were implemented.

In the well-known On-Off Keying (OOK) modulation of Fig. 4(a) the sinusoidal carrier is multiplied by a unipolar NRZ signal, so the power spectral density (PSD) of the complex envelope can be expressed as

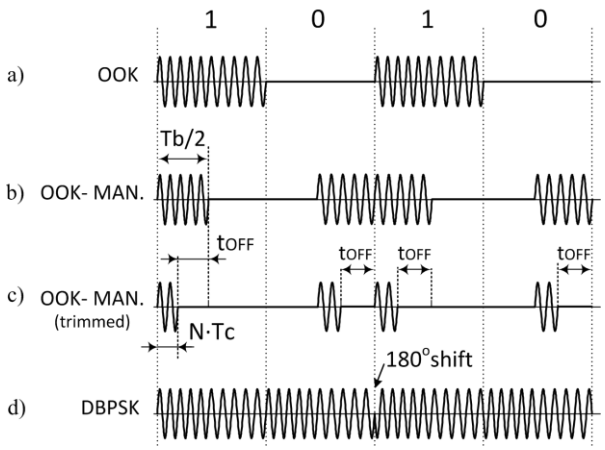

Fig. 4. Waveform diagrams for the tested modulations (the ratio *Tb/Tc* ratio is not realistic, it has been scaled for the sake of clarity).

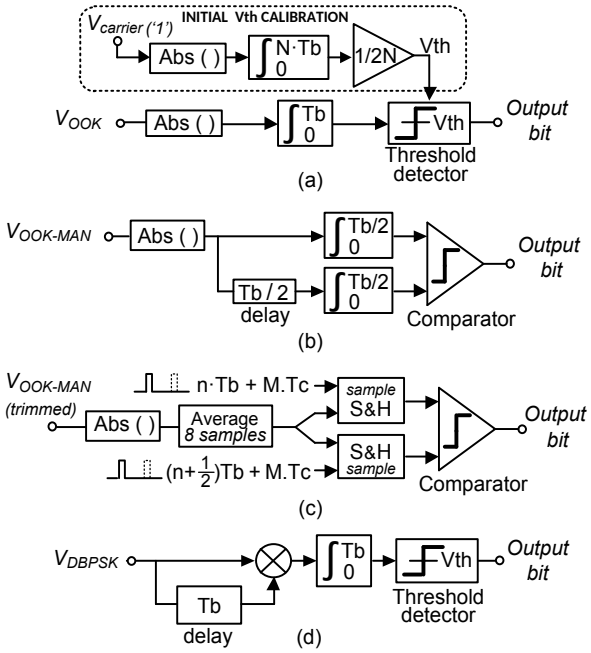

Fig. 5. Detection schemes employed for the tested modulation schemes of Fig. 4. (a) OOK (b) OOK-Manchester (c) trimmed version of OOK-Manchester (d) DBPSK

$$\mathcal{P}_{OOK}(f) = \frac{A_C^2}{2}\left[\delta(f) + T_b\left(\frac{\sin \pi f T_b}{\pi f T_b}\right)^2\right] \quad (1)$$

where A_C is the carrier amplitude and T_b is the bit period [30]. The null-to-null BW of the resulting *sinc* shape is $2/T_b$. The corresponding detection scheme is shown in Fig. 5(a): the optimal threshold value V_{th} is calculated by a calibration routine during 16 bit periods, assuming equally likely '1' and '0'. Then the absolute value of the received signal is integrated during T_b and compared to V_{th} to get the received bit.

In order to improve robustness against channel variations, the OOK-Manchester modulation of Fig. 4(b) was also tested. This approach, which is equivalent to a band-pass 2-PPM (Pulse Position Modulation), does not require a static threshold value, as bit decision is locally made for each T_b. However, two symbols per bit are needed, leading to a worst-case null-to-null BW of $4/T_b$, which is twice the BW of the

conventional OOK scheme (1). The detection strategy is again based on integration of the received signal. In this case a register is required to store the samples of the first $T_b/2$ to later compare the energy of both half-periods as shown in Fig. 5(b).

A lower computational cost alternative for the detection of the OOK-Manchester signal is shown in Fig. 5(c). In this case, the absolute value of the received samples goes through an 8-sample register, whose average value is sampled twice per bit: in $n \cdot T_b + M \cdot T_c$ and $[(n+1/2) \cdot T_b] + M \cdot T_c$, where T_c is the carrier signal period and n and M are natural numbers. Both sampled values are saved and compared at the end of the bit period to get the transmitted bit. The duration of the transmission has been set to M=10 cycles because it has been experimentally checked that this is the minimum number of periods for reaching a steady amplitude in reception. The trimmed version of the OOK-Manchester signal illustrated in Fig. 4(c) is employed in this case, in order to optimize the transmitted power. Note that the signal power received between the sampling time and the end of the corresponding semi-period (t_{OFF} in Fig.4(c)) would be wasted if the waveform of Fig. 4(b) was employed instead. In summary, this scheme leads to a tradeoff between robustness and simplicity, although a precise clock synchronization becomes critical.

Finally, the Differential Binary Phase Shift Keying (DBPSK) modulation shown in Fig. 4(d) has been implemented. A 180º shift occurs when a '1' is transmitted, while the signal remains unaltered in case of '0'. This differential configuration is preferred in simple communication systems since it allows a partially non-coherent detection [30], yielding the classical topology based on correlation shown in Fig. 5(d). The samples corresponding to two consecutive bit periods are saved in a register and the correlation between both periods is performed. A negative value of this correlation, implies that a 180º phase shift has occurred ('1'). Otherwise, no phase shift has happened ('0'). Both the robustness and the computational cost of this detection method are theoretically higher than for the other detectors of Fig. 5. Concerning BW, the PSD of a BPSK modulation [30], considering the worst case (a 180º phase shift every bit period), is

$$\mathcal{P}_{BPSK}(f) = A_C^2 T_b \left(\frac{\sin \pi f T_b}{\pi f T_b}\right)^2 \qquad (2)$$

which leads to a null-to-null BW of $2/T_b$, as for OOK.

IV. Experimental BER Testing

An experimental comparison of the proposed modulations in terms of BER is performed in this Section. A Xilinx Spartan 3AN board has been used to implement a FPGA-based measurement setup [27] according to the scheme of Fig. 6. The tests are performed on a total of 5000 packages of 1000 bits (5 Mb). Three kinds of measurements have been carried out: BER under parasitic mechanical vibrations, BER under parasitic electrical signals applied to the metal wall and BER vs. bit rate. A Pasco SF-9324 vibrator (shaker) was used to produce the mechanical perturbations. Likewise, the parasitic electrical signals have been directly applied from a waveform generator to the metallic plate. A photograph of the complete experimental setup is shown in Fig. 7. The optimal carrier frequency has been manually set and an input signal of only

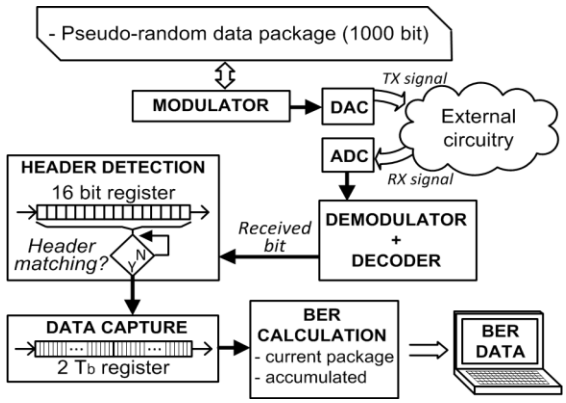

Fig. 6. Block diagram of the software for BER testing.

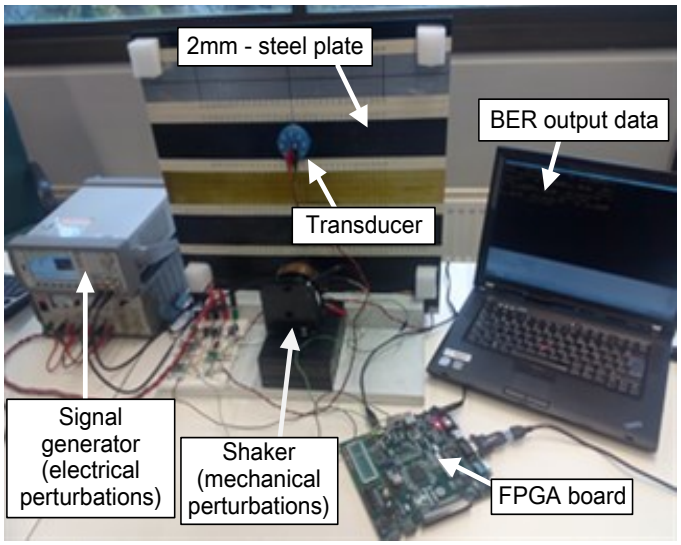

Fig. 7. Photograph of the measurement set-up for BER testing.

100 mV_{pp} has been used for pushing the transducers close to their limit of operation, thus facilitating the BER comparison.

A. BER Under Parasitic Vibrations

A bit rate of 1 kbps has been set to study the BER under the effect of two kinds of mechanical perturbations. On the one hand, a periodic sinusoidal sweeping between 1 Hz and 1 kHz has been applied to cover the typical low frequency vibration range in maritime and ground transport [31]. On the other hand, rectangular pulses with a duration of 5 ms and separated by 250 ms have been generated to study the behavior of the system under higher frequency shocks and continuous rattling.

The first conclusion is that the OOK modulation of Fig. 4(a) (with the detection scheme of Fig. 5(a)) is clearly unsuitable for this application, because of its evident lack of robustness against minimal channel variations that makes the package reception infeasible. Therefore, BER measurements have been limited to the three other systems, whose results are shown in Table I and Table II. Note that the DBPSK modulation (Figs. 4(d) and 5(d)) is clearly the most robust option in both cases followed by the OOK-Manchester with detection based on integrators (Fig. 5(b)). Lastly, the simplified detection system of Fig. 5(c) reveals the worst results.

TABLE I
BER RESULTS WITH LOW-FREQUENCY (1HZ-1KHZ) MECHANICAL VIBRATIONS APPLIED TO THE STEEL WALL

Vin vibrator (Vp)	BER (errors per 1000 bit)		
	OOK-Man. Type 1 (Figs. 4(b) and 5(b))	OOK-Man. Type 2 (Figs. 4(c) and 5(c))	DBPSK (Figs. 4(d) and 5(d))
4	0.124	0.766	0 [1]
5	1.192	3.404	0 [1]
6	>5	>5	0.015
7	No Data [2]	No data [2]	>5

TABLE II
BER RESULTS WITH MECHANICAL PULSES WITH DURATION OF 5MS APPLIED TO THE STEEL WALL

Vin vibrator (Vp)	BER (errors per 1000 bit)		
	OOK-Man. Type 1 (Figs. 4(b) and 5(b))	OOK-Man. Type 2 (Figs. 4(c) and 5(c))	DBPSK (Figs. 4(d) and 5(d))
2	0.011	0.618	0 [1]
3	1.291	3.354	0 [1]
4	3.276	>5	0 [1]
5	>5	No data [2]	0.128
6	No data [2]	No data [2]	0.713
7	No data [2]	No data [2]	1.103
8	No data [2]	No data [2]	>5

TABLE III
BER RESULTS WITH HIGH-FREQUENCY (100 KHZ - 10 MHZ) ELECTRICAL SIGNALS APPLIED TO THE STEEL WALL

Vin vibrator (Vp)	BER (errors per 1000 bit)		
	OOK-Man. Type 1 (Figs. 4(b) and 5(b))	OOK-Man. Type 2 (Figs. 4(c) and 5(c))	DBPSK (Figs. 4(d) and 5(d))
0.4	0 [1]	0.785	0 [1]
0.5	0 [1]	1.101	0 [1]
0.6	0 [1]	>5	0 [1]
0.9	0.163	No data [2]	0 [1]
1	1.357	No data [2]	0 [1]
1.1	>5	No data [2]	0 [1]
1.2	No data [2]	No data [2]	0.007
1.3	No data [2]	No data [2]	3.163
1.4	No data [2]	No data [2]	>5

[1] 'BER=0' strictly equals to BER < $2 \cdot 10^{-7}$ (test performed over 5 Mbit).
[2] 'No data' fields indicate that a smooth transmission could not be reached.

B. BER Under Parasitic Electrical Signals

Two kinds of parasitic electrical chirp have been applied to the metallic wall for this experiment: large-amplitude low-frequency signals (amplitude of 20 V_{pp} and frequency sweep between 0.1 Hz and 1 kHz) and high- frequency signals (chirp between 100 kHz and 10 MHz with variable amplitude). The purpose of the low frequency perturbations is to produce large electrical fields, thus emulating parasitic effects such as electrostatic charge and electrical drifts. On the other hand, the higher frequency chirp aims to model the effect of possible coupling from electrical sources present in the means of transport. Moreover, parasitic signals of several MHz can also be generated from surrounding radiation due to the antenna effect of the whole cargo container (or stack of containers). The bit rate has been set again to 1 kbps.

The measurement results concerning low-frequency perturbations conclude that the system is highly robust against slow voltage variations, even if large amplitudes are applied. No bit errors have been obtained both for the DBPSK scheme of Fig. 5(d) and for the OOK-Manchester detector based on integration of Fig. 5(b), while a BER below 10^{-6} has been measured for the system of Fig. 5(c). However, a more harmful effect has been evidenced for high frequency perturbations. As can be seen from Table III, the evolution of the different systems is very similar to the scenario with mechanical vibrations despite of the different nature of the interference. Once again, the DBPSK scheme clearly yields the best results, followed by the two OOK-Manchester detectors. Note that the relative performance of the simple system of Fig. 5(c) versus the configuration of Fig. 5(b) is poorer than under mechanical parasitic signals.

C. BER versus Bit Rate

A study of the maximum bit rate for the three detection schemes of Fig. 5(b), Fig. 5(c) and Fig. 5(d) has been performed in absence of parasitic perturbations in order to characterize the channel limits in an ideal environment. Under these conditions, an error-free transmission of the 5 Mbit test data has been carried out successfully at 3.5 kbps for the DBPSK scheme, while bit errors appear for the OOK-Manchester at bit rates higher than 2 kbps when the detector of Fig. 5(b) is employed. The alternative of Fig. 5(c) works with no errors for low bit rates of 1-1.5 kbps, but the communication becomes precarious for higher bit rates, collapsing at 2 kbps approximately.

V. PROPOSED LOW-POWER LOW-RATE DIGITAL DBPSK MODULATOR

The previously tested DBPSK scheme (Figs. 4(d)-5(d)) has demonstrated to be the most suitable modulation for the proposed ultrasonic channel due to its good tradeoff between robustness and computational cost.

On this basis, the digital DBPSK modulator shown in Fig. 8 is proposed in this Section. This idea exploits the highly selective bandpass frequency response of the ultrasonic channel (see Fig. 3(a)), which leads to a pseudo-sinusoidal shape at reception when a square carrier is employed in transmission. The filtering out of the high frequency components by the channel implies an inherent energy loss, but some important advantages are obtained in exchange:

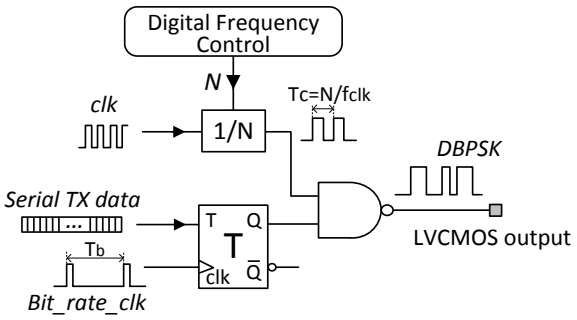

Fig. 8. Proposed DBPSK digital modulator using a square signal from a LVCMOS output port.

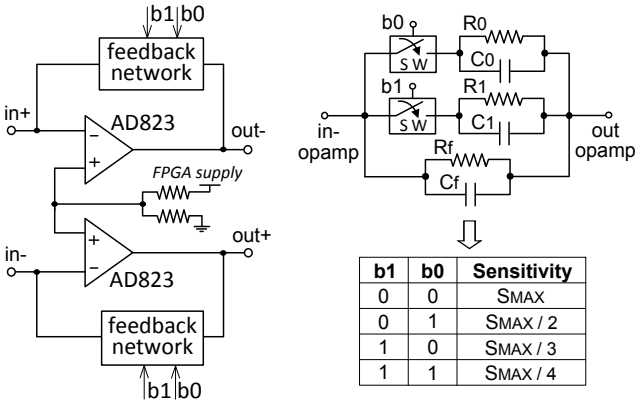

b1	b0	Sensitivity
0	0	SMAX
0	1	SMAX / 2
1	0	SMAX / 3
1	1	SMAX / 4

(a) (b)

Fig. 9. Proposed pseudo-differential charge amplifier with programmable sensitivity (a) General schematic (b) Detail of feedback network and sensitivity values.

1) The typical DAC block [16, 17] becomes unnecessary, reducing cost and power consumption. Moreover, a simple DBPSK modulator using a digital carrier can be implemented by means of a T-type flip-flop and a NAND gate, as illustrated in Fig. 8.

2) Despite the aforementioned amplitude constraints, the carrier frequency resolution is multiplied by the number of cycles required by the DAC for generating an analog sample (64 cycles in the current on-board DAC). This resolution enhancement may become essential in such a reverberant channel with frequency peaks and valleys separated by a few hundred Hz, as seen in Fig. 3(b). Specifically, any frequency given by f_{clock} / N can be generated, where f_{clock} is the frequency of the board clock and N is a natural number.

3) Due to the low-voltage low-power operation, the transmitter PT can be directly driven by the digital output of the FPGA board, thus making unnecessary the use of power amplifiers [22-25] or other driving devices [19, 26]. Typically, the LVCMOS ports of common digital devices are able to source up currents of tens of mA, which clearly fulfills the requirements of the transmitter PT. Concerning the amplitude of the square carrier, a number of voltage levels for the LVCMOS buffers have been defined by the standards of the Joint Electron Device Engineering Council (JEDEC), decreasing from 3.3 V to less than 1 V.

VI. Improved Communication Using Amplitude and Frequency Tracking

As studied in Section II, one of the challenges of through-wall ultrasonic communication is to deal with the variable and unpredictable channel characteristics. With the aim of alleviating this problem, amplitude and frequency tracking capabilities have been developed for the DBPSK scheme defined in the previous Section.

A. Amplitude tracking using a digitally programmable charge amplifier.

Although charge amplifiers are commonly used in charge-mode sensor interfaces, most of works related to through-wall ultrasonic communication just make use of the own capacitive nature of the PT to convert charge to voltage (shunt amplifier) [9, 16, 18, 20-22, 24], performing subsequently a direct voltage amplification or rectification. The main drawback of this voltage mode scheme is its strong dependence on the parasitic impedance of the sensor, which may present a large spread due to fabrication tolerances and temperature. Moreover, sensitivity cannot be modified without affecting BW and noise. In contrast, when using a charge amplifier the input charge is almost completely transferred to the feedback capacitor, so the output voltage is directly proportional to the charge and inversely proportional to the capacitance value. Nonetheless, the use of charge amplifiers in the related literature is limited to the basic topology employed in [25].

In this connection, the digitally-programmable charge amplifier shown in Fig. 9(a) has been designed for both providing signal conditioning and sensitivity tunability. It is based on the Analog Devices AD823 FET-input opamp mounted on a prototype board and supplied by the FPGA 3.3 V supply voltage. A pseudo-differential configuration using two amplifiers has been employed [29]. This configuration

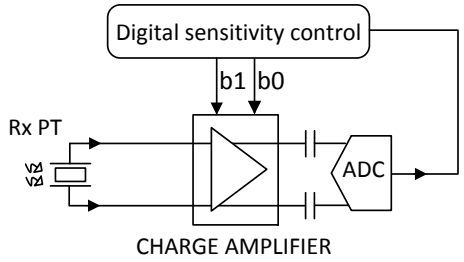

Fig. 10. Block diagram of the proposed output amplitude tracking system

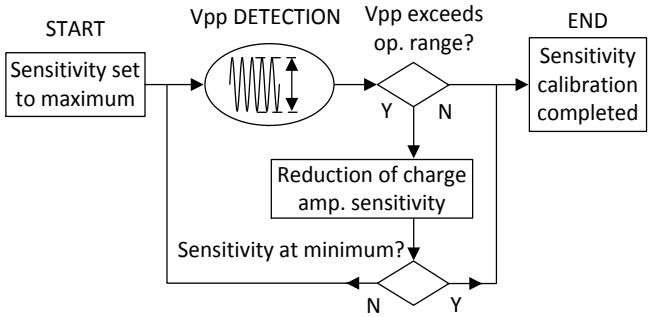

Fig. 11. Flow diagram of the proposed output amplitude tracking system

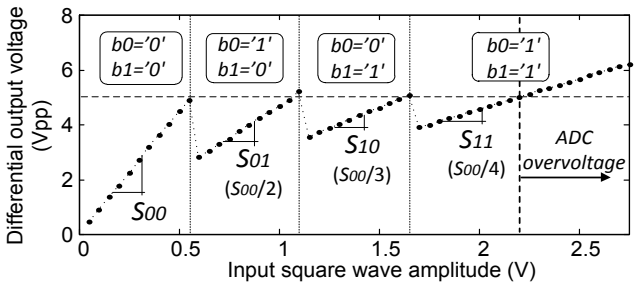

Fig. 12. Validation of the output amplitude tracking system: differential voltage at the output of the charge amplifier versus the input square wave amplitude (rising sweeping from 0 to 2.7 V).

doubles the sensitivity and enhances the rejection of common mode parasitic signals, at the expense of also doubling power consumption. The digitally-programmable RC network of Fig. 9(b) has been used for sensitivity tuning.

The sensitivity S of a charge amplifier is inversely proportional to the feedback capacitance C_{FB} ($S=1/C_{FB}$), yielding a high-pass response with a cutoff frequency $f_C=1/(2\pi C_{FB}\cdot R_{FB})$, where R_{FB} is the feedback resistance. The capacitor C_f has been set to 10 pF, while C_0 and C_1 have been empirically chosen to divide the maximum sensitivity (b_0=b_1='0') by 2 (b_0='1'and b_1='0'), by 3 (b_0='0'and b_1='1') or by 4 (b_0=b_1='1'). Finally, R_0 and R_1 have been properly set to keep f_C approximately constant at 15 kHz.

The charge amplifier programmability has been exploited to design an amplitude tracking system in reception, in order to maximize the output signal without exceeding the ADC input range. The corresponding block diagram is shown in Fig. 10, while the flow diagram of the algorithm is provided in Fig. 11. It has been digitally implemented by using the Xilinx Spartan 3AN board ant the on-board ADC LTC1407A-1 also employed in Section IV. The sensitivity is set to its maximum by default (b_0=b_1='0') and the peak-to-peak value of the received signal is digitally measured. If an overvoltage is detected at the ADC input, the sensitivity is reduced. This procedure is repeated until the signal is within the valid range or the minimum sensitivity is reached.

This tuning technique has been experimentally validated by manually increasing the voltage level at the input transducer in steps of 50 mV up to 2.7 V, leading to the results shown in Fig. 12. The differential output voltage is plotted versus the input square signal. Note that the sensitivity switches down each time the ADC maximum input range is reached, which corresponds to 5 V_{pp} at the differential output.

B. *Frequency tracking*

As previously mentioned, the choice of the optimal transmission frequency in a reverberant channel becomes a challenging task. Chirp signals, widely employed in acoustic imaging for decades [32], have been applied in through-wall ultrasonic communication in [22] for ensuring at least a part of the power to be transmitted at favorable frequencies, at the expense of power efficiency. In contrast, a frequency and amplitude tracking algorithm was used in [18] for establishing the optimal frequency for power and high-rate data transmission. In this reference, a frequency sweep is also performed exploiting the accurate frequency tunability of the digital carrier, but the low-power low-voltage approach of our proposal implies additional constraints with respect to [18]. Firstly, the amplitude of the transmitted signal cannot be adapted, as it comes directly from a digital LVCMOS output. Secondly, the maximum amplitude at reception is also limited, since amplitudes larger than 2.5 V_{pp} would exceed the ADC range.

Assuming this, a system for optimal transmission frequency tracking has been implemented. Its block diagram and flow chart are shown in Fig. 13 and Fig. 14 respectively. A frequency sweep is performed in steps of a predefined duration (T_{test} =100 ms by default). The absolute value of the received signal is integrated (summed) and the maximum power frequency f_{opt} is returned to the transmitter. Note at this point that a two-way communication would be required in practice to return the f_{opt} value to the transmitter, but it would require a high level development of a two-way communication with the corresponding development of communication protocols and hardware duplication, which is out of the scope of this work.

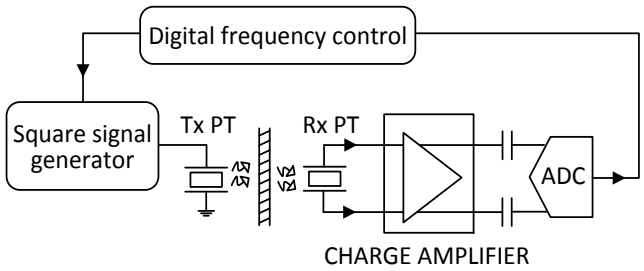

Fig. 13. Block diagram of the proposed tracking system for optimal transmission frequency.

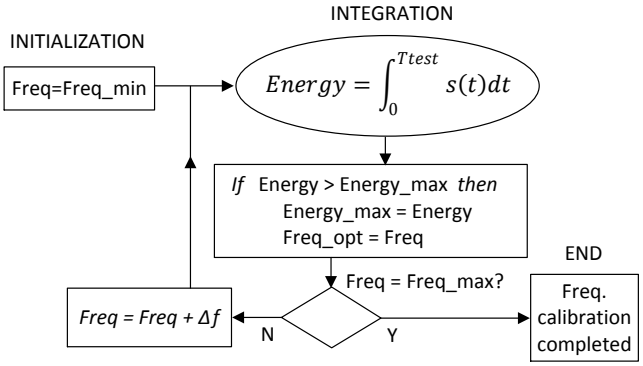

Fig. 14. Flow diagram of the proposed tracking system for optimal transmission frequency.

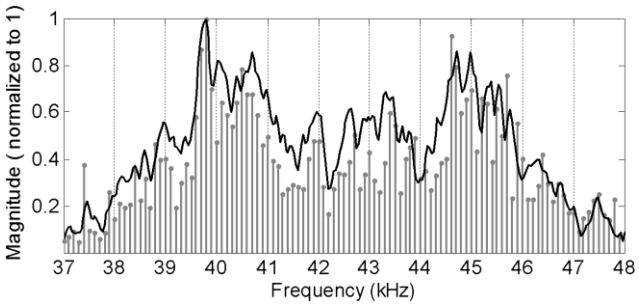

Fig. 15. Application example of the proposed frequency tracking algorithm. Frequency response measured by a spectrum analyzer (black) and normalized energy given by the frequency tracking algorithm at every tested frequency (grey bars).

In order to prove the validity of the optimal frequency tracking algorithm, a linear frequency sweep with steps of approximately 100 Hz (and a integration time of T_{test} =100 ms per step) has been performed between 37 kHz and 48 kHz, using a 0.9 V input square signal. The integration results have been saved for every tested frequency, leading to the graph of Fig. 15. The normalized energy has been plotted in grey bars, while the black solid line is the channel frequency response given by a network analyzer for comparison. Note that an optimal frequency of 39.8 kHz is obtained in both cases, and both measurements follow similar tendencies only differing in a scale factor.

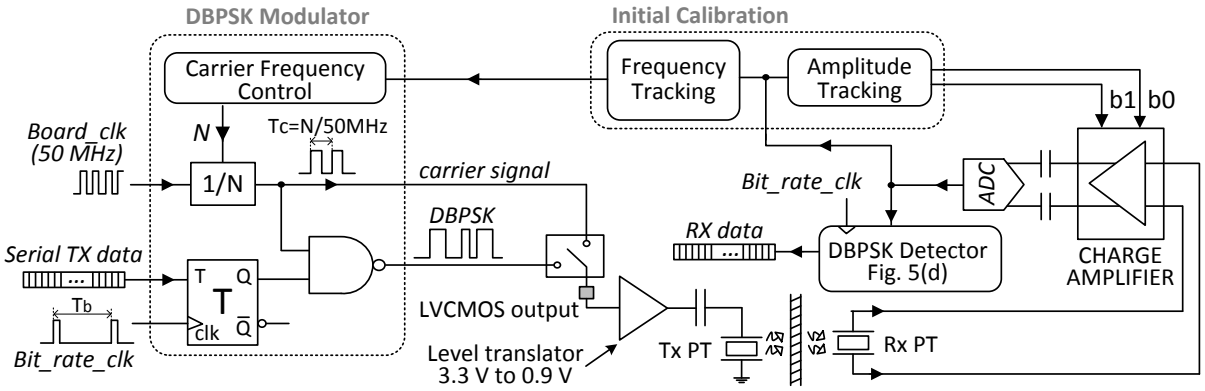

Fig. 16. Complete block diagram of the implemented through-metal communication system including the presented contributions.

VII. Complete Front-End Architecture

A complete front-end diagram including the contributions presented in the previous Sections is shown in Fig. 16. The whole digital circuitry and algorithms have been FPGA implemented. The frequency tracking block controls the carrier frequency of the digital DBPSK modulator, which provides two selectable outputs: the carrier signal, for calibration purposes, and the DBPSK signal for the subsequent data transmission.

A 900 mV square carrier has been employed. This value has been arbitrarily chosen for power efficiency reasons according to the LVCMOS09 JEDEC standard. However, the voltage levels of the digital ports could not be set below 2.5 V in the employed board, so an extra level translator was employed to convert the voltage level to 0.9 V. However, this adaptation does not affect the subjacent idea, as typically LVCMOS buffers can source up currents of tens of mA, clearly higher than the current signal applied to the transmitter PT as mentioned in Section V.

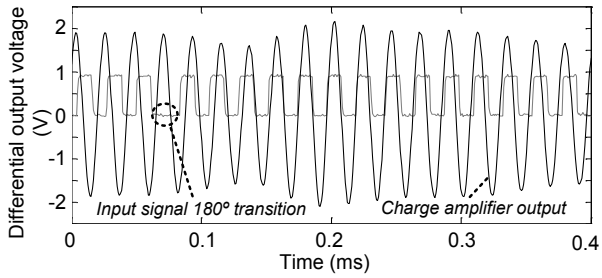

Fig. 17. Transmitted square wave between 0 V and 900 mV and received differential voltage at the output of the charge amplifier.

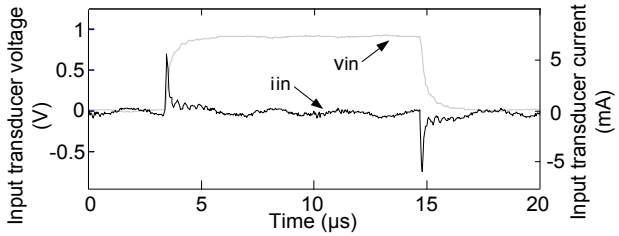

Fig. 18. Transient voltage and current at the input transducer (the square carrier *Vin* is captured before the decoupling capacitor). Current has been measured using the setup of Fig. 2.

Although data rates of 3.5 kbps with a BER < $2 \cdot 10^{-7}$ were achieved in Section IV for the DBPSK scheme of Fig. 5(d), the bit rate of this final system has been set to 1 kbps, both providing enough capacity for container monitoring and extra robustness against environmental hostility.

A. Experimental validation of the front-end

In order to illustrate the operation of the entire system of Fig. 16, a single calibration has been performed once the transmitter and receiver PTs have been placed on the test steel plate. Note that the periodicity with which the calibration process should be performed in a real scenario depends on the transducer fixation quality and the environmental hostility against the PT coupling, so it must be evaluated in each particular case.

Concerning this test, the sensitivity of the charge amplifier has been set to its minimum, and the frequency tracking routine has been executed leading to an optimal frequency of 44.3 kHz. Then, the maximum sensitivity has been set (b_1='0' b_0='0'), which has been subsequently reduced to one half of the maximum value (b_1='0' and b_0='1') by the amplitude tracking algorithm.

The differential voltage at the charge amplifier outputs is shown in Fig. 17 for illustrative purposes, emphasizing the behavior around a 180º phase shifting.

Finally, a capture of the voltage and current waveforms at the input transducer is shown in Fig. 18. Although an input impedance (in magnitude) of 2 kΩ was estimated for the input PT at 40 kHz in Section II, the use of a square carrier involves significant higher frequency components driving a lower impedance due to the capacitive nature of the transducer (note the peak currents associated to voltage edges in Fig. 18). For this reason, the average dynamic power has been calculated applying the integration function of the oscilloscope to the product of both curves of Fig. 18 over one period of the square carrier, leading to a transmitted power of 382 µW.

A report of the experimental results is provided in Table IV together with a summary of related low-rate through-wall ultrasonic communication works. Simple modulation schemes are the preferred option in most cases, as they allow fulfilling low-rate requirements. However, note that a low-power approach in transmission is only feasible for thin walls of few

TABLE IV
SUMMARY OF PUBLISHED LOW-RATE FRONT-ENDS FOR THROUGH-WALL ULTRASONIC COMMUNICATION

Ref.	Transducer Type	Removable Transducer	Transducer Area (mm^2)	Medium Material	Tx Distance (mm)	Input Transducer Power/Voltage	Modulation	Carrier Frequency	Bit Rate
This work	Piezo.	Yes	506	Steel	2	0.9 V [1] - 0.38 mW	DBPSK	≈ 40 kHz	1-3.5 kbps
[25] Hidalgo-Fort 2017	Piezo.	Yes	506	Steel	10	3.3 V	DBPSK	40 kHz	5 kbps
[22] Chakraborty 2015	Piezo.	No	225	Steel	4500 [2]	5 mW	Chirp-OOK	1 MHz	100 bps
[18] Ashdown 2013	Piezo.	No	506	Steel	57.15	> 30 V	AM	1 MHz	30 kbps
[24] Hosman 2011	Piezo.	Yes [3]	487	Steel	N/A [4]	9.6 V_{pp}	MFSK	260-330 kHz	360 bps
[9] Graham 2011	EMAT	Yes	N/A	Steel	25.4 (1'')	1.23 W	QPSK	1 MHz	1 Mbps
[23] Kluge 2008	Piezo.	No	50	Aluminium	7	30 V	AM	3 MHz	1-1.5 kbps
[26] Murphy 2006	Piezo.	Yes [3]	254	Steel	115	20 V_{pp}	DBPSK	1 MHz	5 kbps
[21] Saulnier 2006	Piezo.	No	506	Steel	152.4 (6'')	10 V	AM	1 MHz	0.435 kbps

[1] Square carrier signal
[2] Transversal transmission along a pipeline
[3] Transducers fixed by strapping
[4] Communication between corner posts of abutted cargo containers

millimeters, as the power required for transmission strongly increases for thicknesses of the order of centimeters.

B. Power consumption considerations

The low-power approach presented in this work is focused on the power required by the transmitter transducer (commonly used as a figure of efficiency as can be seen in Table IV) and the simple digital modulation, calibration and detection schemes proposed in the previous Sections. The digital circuitry and software of the system of Fig. 16 have been implemented using the Xilinx Spartan 3AN FPGA board for the sake of versatility, since a complex setup for the BER measurements of Section IV were programmed apart from the final communication system. In fact, other options such as low-power microcontrollers would be a more suitable option for a final whole system implementation in terms of power consumption, given the low computational power requirements.

Despite the above, it is worth it to make some considerations about the power efficiency of the digital part of the system of Fig. 16. Although a precise estimation of the power consumption for FPGA digital circuits is a challenging task [33], the main component of the power consumption is associated to the dynamic power. For a logic gate or connection line, it can be expressed as

$$P_{dynamic} = \propto \cdot C_L \cdot V_{DD}^2 \cdot f_{clock} \quad (3)$$

where α is the average number of transitions between logic levels in one clock cycle, C_L is the load capacitance of the gate, V_{DD} is the supply voltage and f_{clock} is the clock frequency [33]. Note from (3) that the key factor for reducing the power consumption (apart from minimizing the number of logic gates) is to reduce the clock speed requirements as much as possible.

Focusing on the DBPSK modulator of Fig. 8, this novel scheme only requires 5 logic gates to implement the modulator core (a T flip-flop and a NAND gate). Regarding clock speed, an f_{clock} as low as the modulation frequency (~40kHz) is needed, leading to an insignificant power consumption. In contrast, the typical modulator using a DAC would include a relatively complex digital interface for generating the DAC input bits, and a higher clock rate for generating the analog samples would be required. Concerning the square carrier generation, the tuning resolution of the carrier frequency f_c is directly proportional to the board clock frequency f_{clock}, as explained in Section V. Specifically, $f_c = f_{clock}/N$, where N is a natural number, leading to a tradeoff between frequency resolution and power efficiency. Nevertheless, the carrier signal is generated by a simple digital counter, so the resulting power consumption is minimal.

In relation to the receiver digital blocks, the primary interest lies in the sampling rate of the ADC, which strongly affects the power consumption of the DBPSK detector. The precision of the correlation function implemented in Fig. 5(d) increases with the number of samples per period at the expense of a significant increment of the computational cost, mainly due to the multiplication of pairs of digital samples. Thus, it arises a tradeoff between detection robustness and power consumption, which should be weighted in function of the environmental conditions in a real scenario.

VIII. CONCLUSION

A low-power low-rate and low-cost through-wall ultrasonic communication front-end conceived for cargo-container monitoring has been presented in this work. A non-invasive placement method for the piezoelectric transducers based on a customized magnetic case has been employed. Several basic modulation schemes have been tested in terms of BER using a FPGA-based measurement setup. External perturbations have been applied for emulating a real environment. Based on the tests results, a DBPSK modulation using a detector scheme based on correlation has been proved to be the most suitable choice for this application. A compact and efficient digital DBPSK modulator using a square digital carrier has been proposed. A tracking system has been designed to optimize both the transmission frequency and the charge amplifier sensitivity in reception. Bit rates of several kbps can be achieved with a transmitted power lower than 0.4 mW. This low-power approach becomes specially desirable for the transducers placed inside the container, which are typically supplied by means of batteries or energy harvesting sources.

REFERENCES

[1] D. Steenken, S. Voß, and R. Stahlbock, "Container terminal operation and operations research - a classification and literature review," *OR Spectrum,* vol. 26, pp. 3-49, 2004/01/01 2004.
[2] R. Stahlbock and S. Voß, "Operations research at container terminals: a literature update," *OR Spectrum,* vol. 30, pp. 1-52, 2008.
[3] T. Notteboom, "Chapter 2 Strategic Challenges to Container Ports in a Changing Market Environment," in *Research in Transportation Economics* vol. 17, pp. 29-52, 2006.
[4] J. Carn, "Smart container management: Creating value from real-time container security device data," in *2011 IEEE International Conference on Technologies for Homeland Security, HST 2011*, pp. 457-465, 2011.
[5] W. Lang, R. Jedermann, D. Mrugala, A. Jabbari, B. Krieg-Brückner, and K. Schill, "The "intelligent container" - A cognitive sensor network for transport management," *IEEE Sensors J.,* vol. 11, pp. 688-698, 2011.
[6] S. Abbate, M. Avvenuti, P. Corsini, B. Panicucci, M. Passacantando, and A. Vecchio, "An Integer Linear Programming Approach for Radio-Based Localization of Shipping Containers in the Presence of Incomplete Proximity Information," *IEEE Trans. on Intelligent Transportation Systems,* vol. 13, pp. 1404-1419, 2012.
[7] P. Dittmer, M. Veigt, B. Scholz-Reiter, N. Heidmann, and S. Paul, "The intelligent container as a part of the Internet of Things," in *2012 IEEE International Conference on Cyber Technology in Automation, Control, and Intelligent Systems (CYBER)*, pp. 209-214, 2012.
[8] Z. H. D.X. Yang, H. Zhao, H.F. Hu, Y.Z. Sun, B.J. Hou, "Through-Metal-Wall Power Delivery and Data Transmission for Enclosed Sensors: A Review," *Sensors,* vol. 15, pp. 31581-31605, Dec. 2015.
[9] D.J. Graham, J.A. Neasham, and B.S. Sharif, "Investigation of Methods for Data Communication and Power Delivery Through Metals," *IEEE Trans. on Industrial Electronics,* vol. 58, pp. 4972-4980, 2011.
[10] H. Zangl, A. Fuchs, T. Bretterklieber, M. J. Moser, and G. Holler, "Wireless Communication and Power Supply Strategy for Sensor Applications Within Closed Metal Walls," *IEEE Transactions on Instrumentation and Measurement,* vol. 59, pp. 1686-1692, 2010.
[11] E. B. C. Jaskolski, G. Wilhelm, "Magnetic communication through metal barriers," Patent no. wo/2008/039676, Nov. 2007.
[12] D. J. Graham, "Investigation of Methods for Data Communication and Power Delivery Through Metals," School of Electrical, Electronic and Computer Engineering, Newcastle University, September 2011.
[13] S. K. Oruganti, S. H. Heo, H. Ma, and F. Bien, "Wireless energy transfer-based transceiver systems for power and/or high-data rate transmission through thick metal walls using sheet-like waveguides," *Electronics Letters,* vol. 50, pp. 886-888, 2014.
[14] S. Legendre, D. Massicotte, J. Goyette, and T. K. Bose, "Neural classification of Lamb wave ultrasonic weld testing signals using wavelet coefficients," *IEEE Transactions on Instrumentation and Measurement,* vol. 50, pp. 672-678, 2001.
[15] J. Wang, X. Tang, R. X. Gao, L. Duan, and L. Zhang, "On ultrasonic communication through metal structure for machine embedded sensing," *Measurement,* vol. 94, pp. 653-662, 2016.
[16] T. Lawry, "A high-performance system for wireless transmission of power and data through solid metal enclosures," Rensselaer Polytechnic Institute, Troy, New York, 2011.
[17] R. Primerano, "High bit-rate digital communication through metal channels," Electrical, Computer and Systems Engineering Dept., Drexel University, Philadelphia, 2010.
[18] J.D. Ashdown, K.R. Wilt, T. J. Lawry, G.J. Saulnier, D.A. Shoudy, H.A. Scarton, and A.J. Gavens, "A full-duplex ultrasonic through-wall communication and power delivery system," *IEEE Trans. on Ultrasonics, Ferroelec., and Freq. Control,* vol. 60, pp. 587-595, 2013.
[19] M. Bielinski, K. Wanuga, R. Primerano, M. Kam, and K. R. Dandekar, "Application of Adaptive OFDM Bit Loading for High Data Rate Through-Metal Communication," in *2011 IEEE Global Telecommunications Conference - GLOBECOM*, pp. 1-5, 2011.
[20] T.J. Lawry, K.R. Wilt, J.D. Ashdown, H.A. Scarton, and G.J. Saulnier, "A high-performance ultrasonic system for the simultaneous transmission of data and power through solid metal barriers," *IEEE Trans. on Ultrasonics, Ferroelec., and Freq. Control,* vol. 60, pp. 194-203, 2013.
[21] G.J. Saulnier, H.A. Scarton, A.J. Gavens, D.A. Shoudy, T.L. Murphy, M. Wetzel, S. Bard, S. Roa-Prada, and P. Das, "P1G-4 Through-Wall Communication of Low-Rate Digital Data Using Ultrasound," in *2006 IEEE Ultrasonics Symposium*, pp. 1385-1389, 2006.
[22] S. Chakraborty, G.J. Saulnier, K.W. Wilt, E. Curt, H.A. Scarton, and R.B. Litman, "Low-power, low-rate ultrasonic communications system transmitting axially along a cylindrical pipe using transverse waves," *IEEE Trans. on Ultrasonics, Ferroelectrics, and Frequency Control,* vol. 62, pp. 1788-1796, 2015.
[23] M. Kluge, T. Becker, J. Schalk, and T. Otterpohl, "Remote acoustic powering and data transmission for sensors inside of conductive envelopes," in *2008 IEEE Sensors*, pp. 41-44, 2008.
[24] T. Hosman, M. Yeary, and J. K. Antonio, "Design and Characterization of an MFSK-Based Transmitter/Receiver for Ultrasonic Communication Through Metallic Structures," *IEEE Trans. on Instrumentation and Measurement,* vol. 60, pp. 3767-3774, 2011.
[25] E. Hidalgo-Fort, J.R. Garcia-Oya, F. Muñoz-Chavero, and R.G. Carvajal, "Intelligent Containers Based on a Low-Power Sensor Network and a Non-Invasive Acquisition System for Management and Tracking of Goods," *IEEE Trans. on Intelligent Transportation Systems,* vol. PP, pp. 1-6, 2017.
[26] T. L. Murphy, "Ultrasonic Digital Communication System for a Steel Wall Multipath Channel: Methods and Results," Faculty of Rensselaer Polytechnic Institute, New York, 2006.
[27] S.M. Berber, "An automated method for BER characteristics measurement," *IEEE Transactions on Instrumentation and Measurement,* vol. 53, pp. 575-580, 2004.
[28] P. Giannelli, G. Calabrese, G. Frattini, M. Granato, and L. Capineri, "A Buffered Single-Supply Charge Amplifier for High-Impedance Piezoelectric Sensors," *IEEE Transactions on Instrumentation and Measurement,* vol. 68, pp. 368-376, 2019.
[29] M. Massarotto, A. Carlosena, and A. J. Lopez-Martin, "Two-Stage Differential Charge and Transresistance Amplifiers," *IEEE Trans. on Instrumentation and Measurement,* vol. 57, pp. 309-320, 2008.
[30] L. W. Couch II, *Digital and Analog Communication Systems*, Ed. Pearson, 2013.
[31] E.A. Lahti, S.B. Ross, S.T. Maheras, "Transportation Shock and Vibration Literature Review," *University of North Texas Libraries, Digital Library,* DOI: 10.2172/1083410, June 6, 2013.
[32] M. Siegal, "Measurement issues in quantitative ultrasonic imaging," in IEEE Transactions on Instrumentation and Measurement, vol. 47, no. 6, pp. 1435-1438, Dec. 1998.
[33] R. Jevtic, C. Carreras, "Power Measurement Methodology for FPGA Devices," in IEEE Transactions on Instrumentation and Measurement, vol. 60, no. 6, pp. 237 - 247, Jan. 2011

José María Algueta Miguel was born in Hecho, Huesca, Spain. He received the Telecommunications Engineering and Ph.D. degrees from the Public University of Navarra, Spain, in 2008 and 2012 respectively. Currently, he is a researcher with the same university. He has been an invited researcher with the University College Dublin (UCD), Dublin, Ireland, in 2011, with the New Mexico State University, Las Cruces (NM), USA, in 2013, and with the Instituto Nacional de Astrofísica, Óptica y Electrónica (INAOE), Puebla, Mexico, in 2015. His research interests are related to low-power low-voltage analog design, mixed-mode circuits and signal processing, and sensor interfaces.

José Ramón García Oya was born in Seville, Spain. He received the Telecommunications Engineering, Master in Electronics, Signal Processing and Communications and Ph.D. degrees from the University of Seville, Spain, in 2007, 2008 and 2013 respectively. Since 2007, he has been with the Electronic

Engineering Group, Department of Electronic Engineering, University of Seville, where currently he is assistant professor. He has been an invited researcher in the University of Grenoble, France, in 2010, the University of Calgary, Canada, in 2011, the University of Massachusetts Amherst, USA, in 2013, and the University of Paris Saclay, France, in 2017. His research interests include sub-sampling based receivers, multi-standard data acquisition systems, compressive sensing techniques, and ultrasonic communication systems for IoT applications.

Antonio J. López Martín (M'04, SM'11) received the M.S. and Ph.D. degrees (with honors) from the Public University of Navarra, Pamplona (Spain) in 1995 and 1999, respectively. He has been a visiting professor with the New Mexico State University, Las Cruces, NM, and an invited researcher with the Swiss Federal Institute of Technology (ETH), Zurich. Currently, he is Research Director and Professor with the Public University of Navarra and an Adjunct Professor with the New Mexico State University. His research interests include wireless transceivers and sensor interfaces with emphasis on low-voltage low-power implementations. He has published more than 425 technical contributions in books, journals, and conferences. He also holds 6 international patents, leads various research projects and is consultant for local companies.

Dr. Lopez is currently Chair of the IEEE CASS Spain Chapter. He was an Associate Editor of the IEEE TRANSACTIONS ON CIRCUITS AND SYSTEMS-II: EXPRESS BRIEFS (2006-2007) and the IEEE TRANSACTIONS ON CIRCUITS AND SYSTEMS-I: REGULAR PAPERS (2008-2009). He is also in the technical committee of several conferences. He received the Talgo Technological Innovation Award in 2012, the ANIT's Engineer of the Year Award in 2008, the Caja Navarra Research Award in 2007, the Young Investigator Award from the Complutense University of Madrid in 2006, the 2005 IEEE TRANSACTIONS ON EDUCATION Best Paper Award, and the European Center of Industry and Innovation (CEIN) Award in 2004 for excellence in transfer of research results to industry.

Carlos A. de la Cruz Blas received the M.Sc. degree in electronic engineering from the Instituto Nacional de Astrofísica Óptica y Electrónica (INAOE), Puebla, México, and the Ph.D. degree (with honors) in electrical engineering from the Public University of Navarra, Pamplona, Spain, in 1999, and 2004, respectively. In 2006 he was an invited researcher in the School of Electrical, Electronic and Mechanical Engineering at University College Dublin, Ireland. Currently, he is an Associate Professor at the Public University of Navarre. His research interests include low-voltage analog, mixed-mode integrated circuits, instrumentation, sensors, and nonlinear circuits.

Fernando Muñoz Chavero (M'05) was born in El Saucejo, Sevilla, Spain. He received the Telecommunications Engineering and Ph.D. degrees from the University of Seville, Seville, Spain, in 1998 and 2002, respectively. Since 1997, he has been with the Department of Electronic Engineering, School of Engineering, University of Seville, where he has been an Associate Professor since 1999. In 2000 and 2002, he was a Visiting Researcher at Natlab, Philips Research, Eindhoven, The Netherlands, and in 2003, in the Klipsch School of Electrical Engineering, New Mexico State University, Las Cruces. His research interests are related to low-voltage low-power analog circuit design, analog-digital and digital-analog conversion, and analog and mixed-signal processing.

Eduardo Hidalgo Fort received the Telecommunications Engineering Degree and the Master in Electronics, Communications and Signal Processing in 2011 and 2013, respectively, from University of Seville. Since 2010 he has been working in the Electronic Department of University of Seville. In 2012 he was visiting researcher in LCIS-Grenoble INP (Laboratoir de Conception et d'Integration des Systemes) for 4 months and he was visiting researcher in CERN for 2 months in 2017. He has worked and researched about sensors networks, data acquisition, data collection and data integration in large database or platforms like Fiware. He is currently working towards his PhD. His interests are related to sensor networks, data integration and systems for wireless communications.